# A Case Study for Evaluation of Landslide Volume and Two-Dimensional Slope Stability Numerical Simulation Subject to Rainfall Infiltration

J.W. Chen, F.C. Huang, H.P. Wu, W.Z. Liu & C.Y. Chen

*Research and Technology Development Team, Soil and Water Conservation Bureau Council of Agriculture, Executive Yuan, Nantou, Taiwan*

ABSTRACT: A landslide disaster was caused by 0613 torrential rainfall in 2017, which is located at Nantou, Taiwan. The field was investigated by unmanned aerial vehicles (UAV) to collect the spatial information. According to the post-disaster information, the orthophoto and digital surface model (DSM) were produced and used to map the landslide zone. Afterward, the different periods of digital terrain model (DTM) were compared to evaluate landslide volume. Moreover, the numerical analysis program, integrated rainfall-infiltration-slope stability model (IRIS) was selected to simulate landslide. The procedures of IRIS model are divided into three stages. Firstly, the variation of water content is described by Richard's equation, performing finite-element method to solve the process of rainfall-infiltration. Secondly, the concept of limit equilibrium using Janbu's simplified method is utilized for slope stability analysis. Afterward, the critical slip surface is determined by dynamic programming method. The results indicated that using UAV can efficiently observe the variation of micro-photography and evaluate the landslide volume. The application of IRIS model also effectively responded landslide occurrence time and failure slip surface.

## 1 INTRODUCTION

According to climate changing, the frequency of large-scale landslides triggered by typhoon or heavy rainfall was increasing year by year. Furthermore, the influence of rainfall which induced disasters was the infiltration behavior in soil. However, the slopes of residual soil, which were stable during dry season in Taiwan, would be unstable after raining due to the matric suction inside the soil. When heavy rainfall occurred, the rainfall would infiltrate into the slope and increased the saturation of soil. On the opposite side, the matric suction in the soil decreased and made the factor of safety of slope dropped down quickly. Finally, the landslide or debris flow would occur since the slope had been unstable. (Fredlund, 1978; Brand, 1984).

In Taiwan, there were lots of disasters triggered by heavy rainfall, which were caused by typhoons or plum rains during spring and summer. However, these terrible disasters would bring debris flows or landslides which caused damages to humans and buildings. For example, in 2009, there was a terrible typhoon hit Siaolin village, Kaohsiung during summer, which induced a large-scale landslide. Moreover, this disaster event had killed more than 400 people in the village. Also, in 2016, another landslide happened at Hongye village, Taitung induced by typhoon, too. Fortunately, nobody had been killed, but some buildings fell during the landslide. In brief, heavy rainfall, which induces terrible landslides, needs to be concerned more carefully. Furthermore, it's important to do simulations of landslides for government officials to establish an operable standard operating procedure (SOP), which can let them make appropriate decisions for post-disaster survey or remedial measure.

In this study, a landslide occurred at Wushen temple in Nantou will be introduced. In 2017, there was a heavy rainfall in June which was called 0613 torrential rainfall. However, during the torrential rainfall, a landslide near Wushen temple in Guoxing township, Nantou was occurred at 3:00 p.m. on 15$^{th}$ June. According to the precipitation in Changfeng rainfall station, which was the closet rainfall station to Wushen temple, the accumulated rainfall at slope failure time was 275 mm. Besides, for a brief estimation of this landslide, it was 60 m long, 30 m wide and the landslide volume was around 7,200 m$^3$. Moreover, the average depth equaled 4 m, and deepest depth was 10 m. Although no one had been killed in this disaster, a

check dam, which located at toe of this landslide, had been buried. The image after landslide is shown in Figure 1. Hence, it's important for government to clarify the reason of landslide and make operable decisions for remedial measure.

In order to establish a post-disaster survey report, an unmanned aerial vehicles (UAV) has been used to investigate and measure the spatial information of this landslide. Afterward, a digital surface model (DSM) would be produced and used to map the landslides zone. Moreover, the numerical analysis program, integrated rainfall-infiltration-slope stability model (Tsutsumi, 2008), was selected to simulate landslide.

Figure 1. The disaster orthophoto after landslide in 2017 (Nantou Branch, Soil Water Conservation Bureau, Council of Agriculture, Executive Yuan 2017)

## 2 METERIALS AND METHODS

### 2.1 *Post-disaster surveys*

To investigate the disaster situation, an unmanned aerial vehicles (UAV) is selected to build the three-dimensional model, orthophoto and digital surface model (DSM). In this study, the UAV Phantom 4 Professional has carried out a mission for 0613 torrential rainfall. Furthermore, the images have been recognized since the mission. To increase the qualities of image resolution, UAV in this mission has also taken many route plans with different elevation as shown in Figure 2. However, the resolutions of image are much finer than before. Besides, to calibrate the elevation of terrain model, the ground control points around the disaster area are simultaneously set in 4 places to be the characteristic points as shown in Figure 3. Furthermore, Bentley Context Capture version 4.0 is used to feature the points of the aerial photos by aerotriangulation and produce the three-dimensional model, and DSM which has the grid size in 0.02 m.

In brief, the scales and details of this disaster is shown in the images taken by UAV as shown in Figure 4. As the images presented, the slip surface of this landslide seems pass through the bedrock since some weathered shale or sandstone of the landslide have been exposed. However, this surmise will be selected to assume the location of bedrock for numerical simulation in this study.

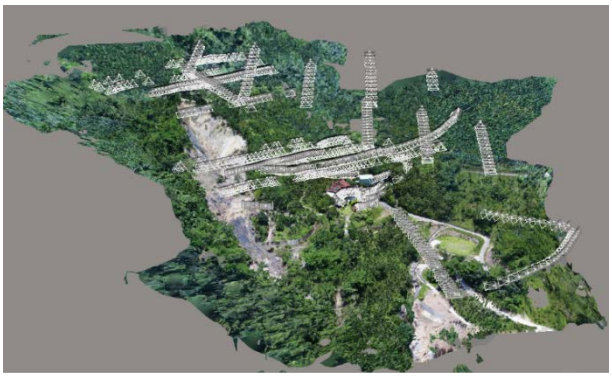

Figure 2. The route of planning with different elevation

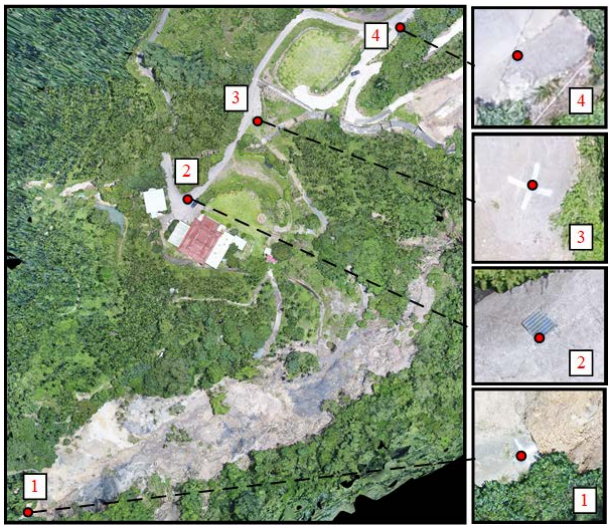


Figure 3. The ground control points in this study

Figure 4. The location of exposed rocks in landslide

## 2.2 *Landslide simulation methods*

In this study, the integrated rainfall-infiltration-slope stability (IRIS) model, which was developed by Tsutsumi (2008), is selected to simulate the landslide situation subject to rainfall infiltration. Furthermore, the model is divided into three stages. First, the Richard's equation is selected to simulate the infiltration and water flow in the soil. Besides, to estimate the process of rainfall-infiltration which induces the increment of water content, finite element method is chosen. However, the results of infiltration analysis are then used to conduct a slope stability analysis simultaneously. Further, The simplified Janbu's method and dynamic programming (DP) method is selected to determine the factor of safety and the critical slip surface. The flow chart of IRIS model simulation steps is shown in Figure 5. In addition, the detail of the simulation steps will be shown below.

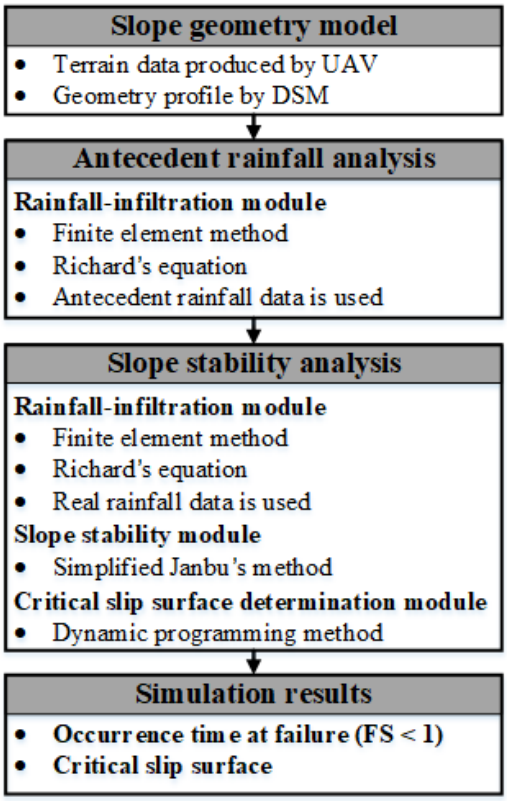


Figure 5. The flow chart of IRIS model simulation

### 2.2.1 *Rainfall-infiltration module*

For IRIS model, the Richard's equation is selected to simulate the infiltration inside the soil. Furthermore, equation of the variation of water content is shown as Equation 1.

$$C(\psi)\frac{\partial \psi}{\partial t} = \nabla \cdot \left\{ K(\psi)\left[\nabla(\psi + z)\right]\right\} \quad (1)$$

where $C(\psi)$ is the soil water capacity, $K(\psi)$ is the hydraulic conductivity, and $\psi$ is the capillary pressure. The lognormal model (LN model) proposed by Kosugi (1996) can be used to represent $C(\psi)$ and $K(\psi)$ for unsaturated conditions ($\psi < 0$) as shown in Equation 2 and Equation 3 separately.

$$C(\psi) = \frac{d\theta}{d\psi} = \frac{\theta_s - \theta_r}{\sqrt{2\pi}\sigma(-\psi)} \exp\left\{ -\frac{\left[\ln(\psi/\psi_m\right]^2}{2\sigma^2} \right\} \quad (2)$$

$$K(\psi) = K_s \left[ Q\left( \frac{\ln(\psi/\psi_m)}{\sigma} \right) \right]^{1/2} \left[ Q\left( \frac{\ln(\psi/\psi_m)}{\sigma} + \sigma \right) \right]^2 \quad (3)$$

where $\theta_s$ is the saturated soil water content, $\theta_r$ is the residual soil water content, $\psi_m$ is the pressure potential corresponding to the median soil pore radius, $\sigma$ is a dimensionless parameter related to the width of the pore-size distribution, and $K_s$ is the saturated hydraulic conductivity. Further, the effective saturation will be presented as Equation 4. Besides, the function $Q(x)$ represents the residual normal distribution and can be expressed as shown in Equation 5.

$$S_e = \left( \equiv \frac{\theta - \theta_r}{\theta_s - \theta_r} \right) = Q\left( \frac{\ln(\psi/\psi_m)}{\sigma} \right) \quad (4)$$

$$Q(x) = \int_x^{\infty} \frac{1}{\sqrt{2\pi}} \exp\left( -\frac{u^2}{2} \right) du \quad (5)$$

where $S_e$ is effective saturation. Furthermore, for saturated conditions ($\psi \geq 0$), values are set at $K(\psi) = K_s$ and $C(\psi) = 0$.

However, the mathematical relationships above are difficult to estimate for analytic solution because of its highly non-linear. Hence, this IRIS model selects finite element method to do estimation.

In simulation, this module will be mentioned in two parts, including antecedent rainfall analysis which defines the initial pore water pressure distribution in slope. However, to simulate the initial condition in antecedent rainfall analysis, the pressure heads of soil in slope are assumed as -0.01 m. Besides, the rainfall intensity is assumed as 0.1 mm/h and continued simulating for 300 days (Chen et al., 2014). Therefore, the distribution of pore water pressure in soil is the initial pore water pressure for slope stability analysis.

After antecedent rainfall analysis, the slope stability analysis will be started. For this analysis, it mentions about three modules, including rainfall-infiltration module, slope stability module and critical slip surface determination module. However, the rainfall-infiltration module is using the real rainfall data to simulate the pore water pressure distribution after rainfall event.

### 2.2.2 *Slope stability module*

According to theory of the rainfall-infiltration module, the results will be the pore water pressures for every mesh. Moreover, a slope stability analysis will be built based on the pore water pressures. For this stage, simplified Janbu's method, which is limit equilibrium method, is selected to estimate the factor of safety. Furthermore, simplified Janbu's method is

going to divide the sliding soil body into several vertical slices. Besides, the stress equilibrium will be calculated for each slice. For this method, the factor of safety estimation is shown as Equation 6 and Equation 7 separately.

$$F_s = \frac{\sum A_i}{\sum B_i} = \frac{\sum \left[ c'_i l_i \cos a_i + \left( W_i - u_i l_i \cos a_i \right) \tan \phi'_i \right] / m_a}{\sum \tan a_i} \quad (6)$$

$$m_a = \cos^2 a_i \left( 1 + \frac{\tan a_i \tan \phi'_i}{F_s} \right) \quad (7)$$

where $i$ is the number of each vertical slice, $c_i'$ is the cohesion of soil, $\phi_i'$is the friction angle of soil, $W_i$ is the weight of every vertical slice, $a_i$ is the angle between horizontal and slip surface for each slice, and $l_i$ is the length of slip surface for each slice. Afterward, $u_i$ is the pore water pressure of slip surface for each slice, which is estimated by rainfall-infiltration module. Besides, $A_i$ is the resistance force, and $B_i$ is the driving force.

### 2.2.3 *Critical slip surface determination module*

Based on simplified Janbu's method, the slip surfaces should be assumed in different shapes before estimating the factor of safety. Besides, the critical slip surface is selected by the smallest factor of safety. However, this process is too subjective to estimate a critical slip surface which truly occurred. Hence, this model uses Dynamic Programming method (DP) to estimate the critical slip surface with the smallest factor of safety (Yamagami and Ueta, 1986 ; Baker, 1980). Furthermore, the Dynamic Programming method can only be suitable for additive functions. However, the equation of simplified Janbu's method doesn't correspond to the limitation of Dynamic Programming method. Therefore, another method developed by Baker (1980) has been produced. The method developed by Baker consults the classical calculus of variations and define a new function G as shown in Equation 8.

$$G = \sum_{i=1}^{n} \left( A_i - F_s \cdot B_i \right) \quad (8)$$

where $n$ is the numbers of slice for calculating, $F_s$ is the factor of safety. Besides, $A_i$, $B_i$, and $F_s$ are unknown in the equation. Therefore, the equation should be calculated by iterative algorithms, and started by any value. In this study, the value of factor of safety in the beginning is defined as 1.

Afterward, the relationship between the minimum of function $G$ and the smallest factor of safety has been proved that is equivalent. Hence, the critical slip surface will be selected after estimating the minimum of function $G$. In other words, the critical slip surface is estimated when factor of safety less than 1, which means the slope is unstable.

Moreover, to combine Dynamic Programming method and function $G$, which looks for critical slip surface, should divide the slope into $n+1$ stages as the vertical lines shown in Figure 6(a). Meanwhile, every stage can be divided into several states as the circular points shown in Figure 6(a) (Chen et al., 2014). As shown in Figure 6(b), the line $jk$ can be part of slip surface when $(i,j)$ and $(i+1,k)$ are adjacent to each other. On the opposite side, the quadrangle, which is combined by point $a$, $b$, $k$, and $j$, can be considered as a slice of the slip surface. Furthermore, $A_i$ and $B_i$ can be calculated by Equation 6 and Equation 7 separately. Hence, the variable $DG_i(i,k)$, which starts from $(i,j)$ to $(i+1,k)$, is shown as Equation 9.

$$DG_i\left( j,k \right) = A_i - F_s \cdot B_i \quad (9)$$

Meanwhile, if the function $H_i(j)$ was defined as the minimum path from the first stage to function $G$ of $(i,j)$, Equation 10 will be built. Besides, the boundary condition of the start and terminal points in the path are shown as Equation 11 and Equation 12 separately.

$$H_{i+1}(k) = \min_{j=1\sim S_{n+1}} \left[ H_i(j) + DG_i\left( j,k \right) \right]_{k=1\sim S_{i+1}}^{j=1\sim n} \quad (10)$$

$$H_1(j) = 0, \ j = 1 \sim S_1 \quad (11)$$

$$G_m = \min G = \min_{j=1\sim S_{n+1}} \left[ H_{n+i}(j) \right] \quad (12)$$

where $S_i$ is the number of total layer for the stage of number $i$.

In brief, according to the methods above, the slip surface which has the minimum factor of safety will be estimated firstly. Further, $A_i$ and $B_i$, which is on this slip surface, will be brought back to Equation 6 and the correct factor of safety will be calculated. Note that the critical slip surface is based on the factor of safety less than 1, which means the slope has collapsed.

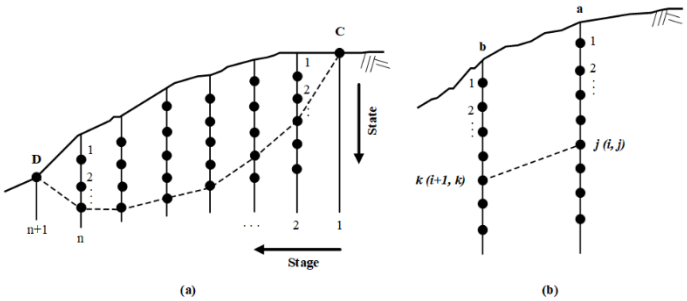


Figure 6. (a) The route of stages to determine critical slip surface by dynamic programming method (b) Determination of signal (Chen et al. 2014)

## 3 NUMERICAL MODEL AND SITE CONDITIONS

In this study, the landslide of Wushen temple, which occurred in 0613 torrential rainfall, is selected. Furthermore, this disaster was located in Guoxing Township, Nantou. However, during 0613 torrential rainfall in 2017, a landslide occurred near the Wushen temple and the accurate failure time is 3:00 p.m. on 15$^{th}$ June. Moreover, to do simulation of this disaster,

the real rainfall data will be collected from Changfeng rainfall station, which is the closet rainfall station to the Wushen temple. Further, the rainfall data will start from 1st May to 17th June as shown in Figure 7. Therefore, the rainfall-infiltration module is selected the rainfall data mentioned above to estimate the pore water pressure distribution in slope stability analysis.

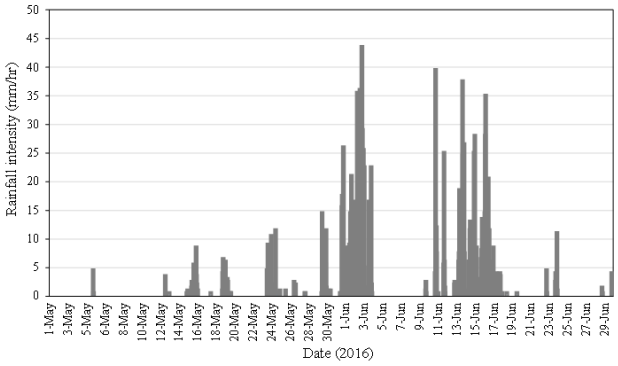


Figure 7. Rainfall intensity from 1st May to 30th June in 2017 (Changfeng rainfall station, 2017)

### 3.1.1 *Geometry model*

For landslide simulation, the IRIS model is estimated the slip surface in two-dimensional. Therefore, the digital elevation model (DEM) in 2011 is used to determine the original slope profile in two-dimensional. However, the aspect map is produced to select a representative profile which is between two different aspects of slope. Hence, the location of profile in this study is shown as Figure 8.

Since the underground condition can't be known easily, the location of bedrock is assumed in this study. As mentioned in post-disaster survey, the slip surface seems passing through the bedrock. Therefore, the location of bedrock is assumed as the deepest depth of landslides which is almost 10 m. In brief, the overall geometry model of this slope is shown in Figure 9.

Figure 8. Location of profile for IRIS model simulation

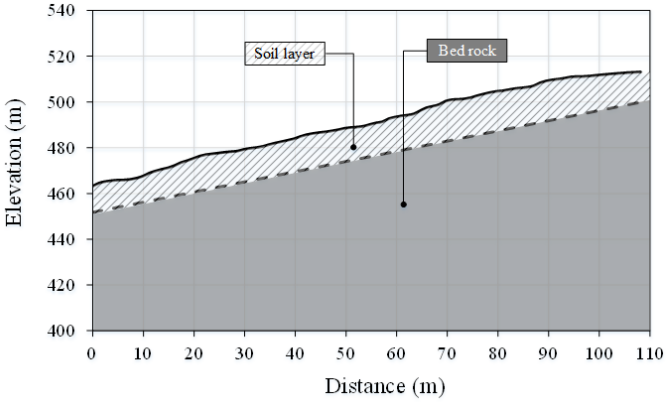


Figure 9. Geometry model for IRIS model simulation

### 3.1.2 *Soil and bedrock propertiess*

As mentioned in section 2.2, to simulate the landslide in IRIS model should not only have rainfall data, but also the parameters of soil. Therefore, the parameters include soil unit weight ($\gamma$), the cohesion of the soil (c'), soil friction angle ($\phi$'), saturated permeability of soil ($k_s$), and the parameters which represent the unsaturated soil mechanic. However, the first step is recognizing the soil type in the disaster area. Instead of doing lab experiment, this study uses geological map, which described types of soil on the map, to recognize the soil type near Wushen temple. After searching on the geological map, the soil type of this area is sandy loam. Moreover, the soil physical and engineering properties for sandy loam is shown in Table 1 (Minnesota Department of Transportation, 2007).

Table 1. The typical soil properties of sandy loam

| Soil properties | | | |
|---|---|---|---|
| | Max. | Min. | Avg. |
| Unit weight, $\gamma$ (t/m$^3$) | 2.04 | 1.73 | 1.89 |
| Cohesion, c' (t/m$^2$) | 2.04 | 1.02 | 1.53 |
| Friction angle, $\phi$' (degrees) | 32 | 25 | 28.5 |
| Permeability, $k_s$ (m/s) | $10^{-4}$ | $10^{-5}$ | $10^{-6}$ |

Although some soil properties have be mentioned above, there is another parameter should be determined. The soil-water characteristic curve (SWCC) of typical sandy loam, which represent unsaturated soil mechanism, is shown as Figure 10 (Carsel and Parrish, 1988). Besides, the parameters of LN model mentioned in section 2.2 for this study are shown as Table 2.

For simplified the model in simulation, this study assumes the bedrock properties are constant. Therefore, the cohesion of bedrock ($c_b$') is 100 t/m$^2$ and the friction angle ($\phi_b$') is 60 degrees. In brief, the properties mentioned above will be the input parameters in IRIS model for this study. However, because of the inhomogeneity and uncertainty in geology, this study tests different values based on the typical properties

of sandy loam for back analysis. The test models of different values have 72 cases as shown in Figure 11.

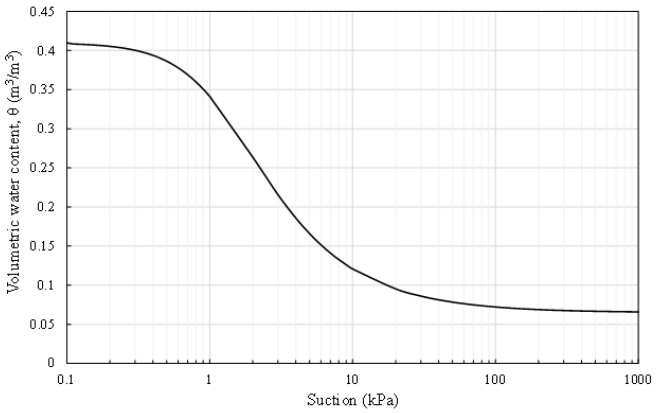


Figure 10. Soil-water characteristic curve of typical sandy loam

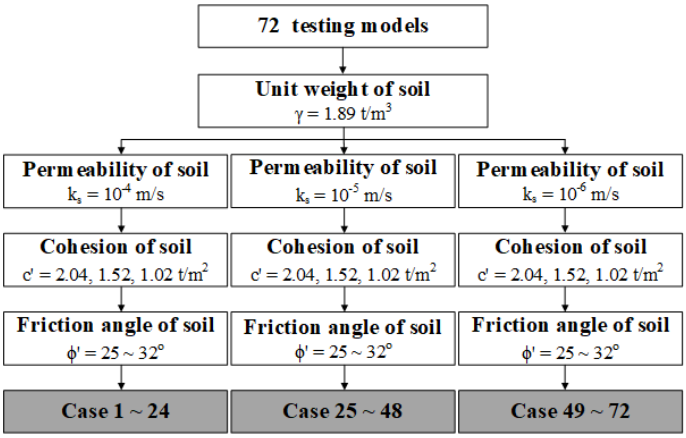


Figure 11. Flow chart for model testing

Table 2. The LN model parameters of sandy loam

| Parameters of LN model | |
|---|---|
| Saturated volumetric water content, $\theta_s$ ($m^3/m^3$) | 0.41 |
| Residual volumetric water content, $\theta_r$ ($m^3/m^3$) | 0.065 |
| $\psi_m$ (cm) | -26.4 |
| σ | 0.486 |

## 4 RESULTS AND DISCUSSION

### 4.1 *Terrain change and volume evaluation*

In this study, the terrain model after the landslide is produced. Furthermore, the profile of landslide, which located at the same place mentioned in section 3.1.1, is shown in Figure 12. However, the slip surface after landslide is selected to be the calibration for simulating the numerical model in this study.

Moreover, the digital elevation model in 2011 which before disaster is used to compare with the digital surface model mentioned in post-disaster survey for estimating the landslide volume. Furthermore, the changes of elevation caused by landslide are determined after comparing. Therefore, the landslide volumes can be estimated by the area and change of height. Besides, the changes of height are shown in Figure 13. After estimating, the area of erosion equals 2,729 $m^2$ and the landslide volume equals 19,278 $m^3$ as shown in Table 3. However, since the erosion area is considered by different reasons and methods, the estimation for landslide volume is larger than the result in rapid report, which is 7,200 $m^3$.

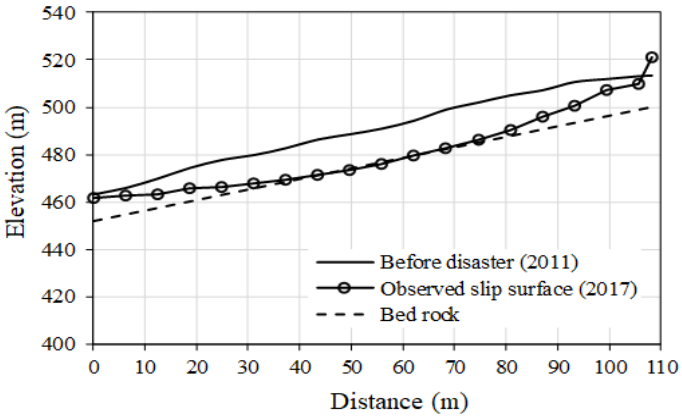


Figure 12. Observed slip surface by UAV survey

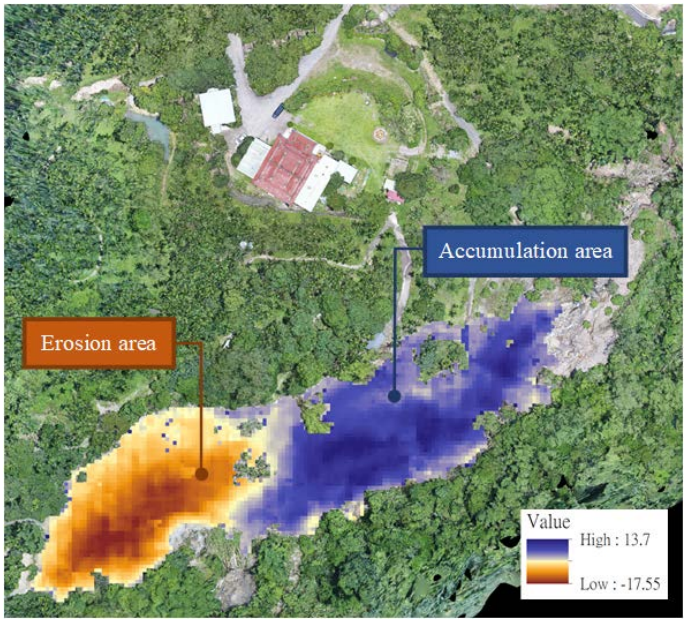


Figure 13. Observed changes of height by UAV survey

Table 3. Estimation of landslide volume

| Depth (m) | Number of grids ($m^2$) | Mean elevation (m) | Volumes ($m^3$) |
|---|---|---|---|
| 0.0 ~ 2.5 | 831 | 1.25 | 1039 |
| 2.5 ~ 5.0 | 443 | 3.75 | 1661 |
| 5.0 ~ 7.5 | 441 | 6.25 | 2756 |
| 7.5 ~ 10.0 | 366 | 8.75 | 3203 |
| 10.0 ~ 12.5 | 375 | 11.25 | 4219 |
| 12.5 ~ 15.0 | 340 | 13.75 | 4675 |
| 15.0 ~ 17.6 | 106 | 16.28 | 17.25 |
| | | Total | 19278 |

### 4.2 *Landslide simulation results*

According to the uncertainty of the soil properties, the back analysis which can describe the real condition in situ is selected in this study. Besides, the main result of IRIS model after simulating is the critical slip surface which occurred at the smallest factor of safety. In other words, the criteria of failure slope is determined when factor of safety is less than 1 in this study. Furthermore, the occurrence time of landslide in IRIS model also can be estimated by the historical rainfall data. In brief, when the simulation date of rainfall data went to the end, IRIS model will stop estimating and return the result of critical slip surface with the smallest factor of safety simultaneously.

Although 72 cases of test models have been estimated, only 15 cases with the factor of safety less than 1, which mean the slope is unstable, are considered as shown in Table 4. Besides, as mentioned in section 3, 1st May is the date that begin to simulate both rainfall-infiltration module and sloe stability module. Hence, those failure cases with occurrence time at 1st May are ignored in this study because that the slopes have been unstable in antecedent rainfall instead of 0613 torrential rainfall.

Table 4. The results after simulating

| Collapse cases in simulation | | | | |
|---|---|---|---|---|
| Case No. | $k_s$ (m/s) | c′ ($t/m_2$) | ϕ′ (degrees) | Occurrence time (-) |
| 58 | $10^{-6}$ | 1.52 | 31 | 2017/06/15 16:50 |
| 59 | $10^{-6}$ | 1.52 | 30 | 2017/05/01 00:00 |
| 60 | $10^{-6}$ | 1.52 | 29 | 2017/05/01 00:00 |
| 61 | $10^{-6}$ | 1.52 | 28 | 2017/05/01 00:00 |
| 62 | $10^{-6}$ | 1.52 | 27 | 2017/05/01 00:00 |
| 63 | $10^{-6}$ | 1.52 | 26 | 2017/05/01 00:00 |
| 64 | $10^{-6}$ | 1.52 | 25 | 2017/05/01 00:00 |
| 65 | $10^{-6}$ | 1.02 | 32 | 2017/05/01 00:00 |
| 66 | $10^{-6}$ | 1.02 | 31 | 2017/05/01 00:00 |
| 67 | $10^{-6}$ | 1.02 | 30 | 2017/05/01 00:00 |
| 68 | $10^{-6}$ | 1.02 | 29 | 2017/05/01 00:00 |
| 69 | $10^{-6}$ | 1.02 | 28 | 2017/05/01 00:00 |
| 70 | $10^{-6}$ | 1.02 | 27 | 2017/05/01 00:00 |
| 71 | $10^{-6}$ | 1.02 | 26 | 2017/05/01 00:00 |
| 72 | $10^{-6}$ | 1.02 | 25 | 2017/05/01 00:00 |

In brief, according to back analysis, the 58th case which has the occurrence time at 16:50 15th June is the ideal model in this study since the estimated occurrence time is close to the current one in situ. In this case, the permeability, the cohesion and the friction angle of soil are $10^{-6}$ m/s, 1.52 $t/m^2$ and 31 degrees separately. Furthermore, the critical slip surface estimated by the IRIS model and observed from post-disaster survey are both shown in Figure 14. After comparing the estimated slip surface with the observed one, the weakest layer seems between the colluvium and the bedrock. However, the scale of estimated slip surface is less than observed one because of the limitation of the IRIS model. For estimating slope stability in IRIS model, the simulation is stopped when the factor of safety is less than 1. On the other words, this model can't simulate the second disaster after the first one occurred. Therefore, the top part of estimated slip surface is higher than observed one.

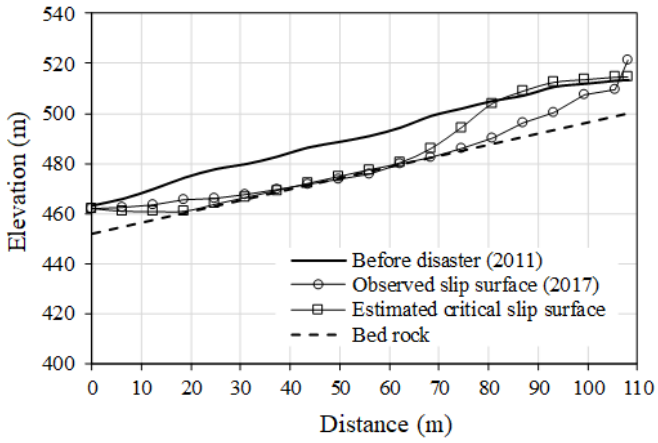


Figure 14. Estimated critical slip surface of simulation

## 5 CONCLUSION

For post-disaster survey, the UAV has been used to investigate the site condition, including the terrain changes and the orthophoto after landslides. Besides, the digital surface model (DSM) have been established for building the geometry model in IRIS model. Furthermore, the landslides volume can be estimated conservatively with the digital terrain model (DTM) which are produced before and after disaster. However, this study gives some distinct procedures for post-disaster survey.

Moreover, after building the geometry model from DSM made by UAV, the IRIS model plays an important role in simulation of landslide. In this study, 72 cases of IRIS model have been tested for back analysis. Although one of the results is fitting not only the occurrence time, but also the critical slip surface in situ, there are some suggestion for this model after testing. In this study, only first disaster is concerned so that the estimated critical slip surface is more conservative than the observed one which may have second or more disaster after the first one occurred. Hence, the model should be updating for its limitation to simulate the landslide continuously. For future works, this study also suggests the soil layer be divided to different layers with different permeabilities for some cases that have deeper depth of soil layer. However, the assumption of different permeabilities may let the simulation of landslide be more conservative and close to reality.

In conclusion, the brief procedures of post-disaster survey and the steps for landslide simulation is suggested in this study. Therefore, these results can establish an operable standard operating procedure

which can help government officials to make appropriate decisions for post-disaster survey and remedial measure of landslide area in the future.

## 6 REFERENCE


Baker, R. 1980. Determination of the critical slip surface in slope stability computations. *International Journal for Numerical and Analytical Methods in Geomechanics*, 4(4), 333-359.

Brand, E.W., Premchitt, J., & Phillipson, H. 1984. *Relationship between rainfall and landslides in Hong Kong (Vol. 1): Proceeding of the Forth International Symposium in Landslides.* Torontom Canada.

Carsel, R. F., & Parrish, R. S. 1988. Developing joint probability distributions of soil water retention characteristics. *Water Resources Research*, 24(5), 755-769.

Chen, C.Y., Fujita, M. & Tsutsumi, D. 2014. The influence of bedrock location and soil characteristics on rainfall-runoff and large-scale landslides. *Journal of Chinese Soil and Water Conservation*, 45 (4): 243-256

Fredlund, D., Morgenstern, N.R., & Widger, R. 1978. The shear strength of unsaturated soils. *Canadian geotechnical journal*,15(3), 313-321.

Kosugi, K. I. 1996. Lognormal distribution model for unsaturated soil hydraulic properties. *Water Resources Research*, 32(9), 2697-2703.

Minnesota Department of Transportation. 2007. *Pavement Design.* USA

Tsutsumi, D., & Fujita, M. 2008. Relative importance of slope material properties and timing of rainfall for the occurrence of landslides. *International Journal of Erosion Control Engineering*, 1(2), 79-89.

Yamakoshi, T., Ishizuka, T., Kaji, A., Ito, Y., Osaka, S., & Nakagome, A. 2012. Quick monitoring tool for landslide dam outburst debris flow and its application to the actual disaster. *In EGU General Assembly Conference Abstracts*, Vol. 14, p. 6882.